



TiO₂-supported Ag nanoclusters with enhanced visible light activity for the photocatalytic removal of NO

Yanyan Duan^{a,b}, Jianmin Luo^b, Shaochen Zhou^b, Xinyou Mao^b, Muhammad Wajid Shah^c, Fu Wang^{b,***}, Zhihong Chen^{a,***}, Chuanyi Wang^{a,b,*}

^a Shenyang Institute of Automation, Guangzhou, Chinese Academy of Sciences, Guangzhou, 511458, China

^b Laboratory of Environmental Science and Technology, The Xinjiang Technical Institute of Physics and Chemistry, Chinese Academy of Sciences, Urumqi 830011, China

^c MOE Key Laboratory of Bioinorganic and Synthetic Chemistry, Lehn Institute of Functional Materials, School of Chemistry, Sun Yat-Sen University, Guangzhou 510275, China



ARTICLE INFO

Keywords:

Supported Ag nanoclusters
Photocatalysis
NO removal
Selective degradation
Visible light

ABSTRACT

Metal nanoparticles have been widely used in photocatalysis, while metal nanoclusters (NCs) smaller than 2 nm are barely studied for photocatalytic reactions. In this work, we explored the photocatalytic performances of the TiO₂ supported Ag NCs (Ag NCs/TiO₂). Interestingly, small loading amount (about 0.89% in Ag/Ti molar ratio) of Ag NCs on TiO₂ (Ag NCs/TiO₂-0.89) results in remarkable improvement in the photoactivity of NO removal. Ag NCs/TiO₂-0.89 can remove 62% of NO in just 7 min, compared to that of only about 20% and 32% for the pristine TiO₂ and Ag NCs, respectively. Besides, the support (TiO₂) exhibits a strong effect, and Ag NCs/TiO₂-0.89 is found to exhibit excellent stability and recyclability. More importantly, the composite can depress the amount of formed intermediate, NO₂. In addition, Ag NCs/TiO₂-0.89 has better photocatalytic performance against rhodamine B and methylene blue (cationic dyes) than methyl orange (anionic dye). This selectivity towards cationic dyes is interpreted by the electronegativity of AgNCs/TiO₂-0.89 (the Zeta potential of which is -12.4 mV). Results also show that Ag NCs can behavior like a semiconductor, responding to the incident visible-light, promoting the separation of photogenerated electron-hole pairs and producing $\cdot\text{O}_2^-$. Both $\cdot\text{O}_2^-$ and photogenerated carriers are responsible for the photocatalytic reactions. The present study expands applications of Ag NCs, and highlights the vital effects of Ag NCs on the enhanced photoactivity and photocatalytic selectivity.

1. Introduction

Recently, metal nanoparticles (NPs) with size larger than 2 nm have been widely used in photocatalysis [1–4]. Metal NPs demonstrate surface plasmon resonance (SPR) effect under suitable light irradiation [5]. Electrons transfer from metal NPs to the conduction band (CB) of the neighboring semiconductor under SPR excitation, which improves the photoactivity of the composites. On the other hand, when the size of metal NPs drops to significantly small range, typically 2 nm or smaller, distinctive properties (includes electronic, chemical, and optical) happen [6]. This is because acute changes emerge with the structural arrangement of metal atoms. And these species are usually called nanoclusters (NCs) or quantum clusters to distinguish them from their NPs counterparts.

Generally, these NCs with molecular-like properties are widely used in chemo-sensing [7], bio-labeling [8], and single-molecule microscopy

[9]. Specially, many reports are focused on the usage of metal NCs for catalysis, for example, Au₂₅(SR)₁₈ used for CO oxidation [10,11], Au NCs for electrocatalytic reduction of oxygen [12], Pd clusters for electrocatalytic water oxidation [13], and Au₅₅ clusters for selective oxidation of styrene [14]. However, few researches are concentrated on the utilization of metal NCs for photocatalysis [15].

With respect to photocatalysts, recyclability is the fundamental element during photocatalytic reactions. NCs with active phase are usually deposited on supports to improve their photocatalytic stability [10,16–18]. Compared with colloidal catalysts, supported catalysts are more robust and easier to recovery. Besides, suitable supports can enhance the photoactivity of the NCs because of the electron-transfer effects between NCs and supports. Some representative data about using supported-metal NCs for photocatalytic purposes are listed here. Yu et al. found that TiO₂ nanocrystals supported-Au₂₅(SR)₁₈ showed enhanced photoactivity for the degradation of methyl orange (MO), and

* Corresponding author at: Shenyang Institute of Automation, Guangzhou, Chinese Academy of Sciences, Guangzhou, 511458, China.

** Corresponding authors.

E-mail addresses: wangfu@ms.xjb.ac.cn (F. Wang), chenzhong1227@sina.com (Z. Chen), cywang@ms.xjb.ac.cn (C. Wang).

the composite exhibited excellent stability in cycle experiments [6]. Sridharan et al. reported that graphitic carbon nitride ($g\text{-C}_3\text{N}_4$) supported-Ag NCs displayed improved photocatalytic degradation activity for methylene blue (MB) and MO dye molecules under visible light, compared to those for the pristine $g\text{-C}_3\text{N}_4$ [19]. Sakai et al. showed that $\text{Au}_{25}(\text{SG})_{18}$ clusters modified TiO_2 electrodes had significant and stable photocurrent. Besides, the incident photon-to-electron conversion efficiency (IPCE) measurement from 400 to 900 nm suggested photo-generated electrons transferred from excited Au_{25} to the CB of TiO_2 [16]. However, studies on photocatalytic removal of NO, as well as selective dye degradation under visible light, through TiO_2 -supported Ag NCs are rarely reported.

Nitric oxide (NO), a kind of significant air contaminant, which mainly stems from inadequate combustion of nitrogenous fuels, vehicle exhaust emissions, and the boiler waste gas. It is the main sources of many environmental problems, such as ozone depletion, acid rain, photochemical smog and so on. Besides, NO is responsible for many diseases, like lung function abnormalities, hyperiron hemoglobin, neurasthenic syndrome, choking sensation in chest, respiratory distress syndrome, and cough etc. Generally, NO is easily combined with O_2 to form NO_2 , which is corrosive and highly toxic. Many approaches can be employed to remove NO, like selective catalytic reduction (SCR) [20], selective non-catalytic reduction (SNCR) [21], filtration [22], and thermal catalysis [23]. But these methods are not efficient for the removal of NO in urban environments, because the concentration of NO in the atmosphere is usually very low, typically at parts per billion (ppb) level [24]. Therefore, alternative method is highly desired to eliminate urban NO. Photocatalysis, which is extensively considered as a “green” technology, can utilize solar light to effectively remove NO in low concentration [25–30]. On the other hand, organic dyes are the dominant organic contaminants in wastewater, which come from textile, printing, and other related industries [31,32]. Photocatalytic degradation of different dyes with high selectivity favors the in-depth exploration of the interaction between dyes molecules and photocatalysts [33].

Herein, Ag NCs were supported on the surface of commercial TiO_2 (P25, contains anatase and rutile), and we also investigated the photocatalytic application of TiO_2 -supported Ag NCs (Ag NCs/ TiO_2) for NO removal. Results illustrate that very limited loading amount (about 0.89% in Ag/Ti molar ratio) of Ag NCs can remarkably improve the photocatalytic activity of NO removal. Moreover, the support (TiO_2) brings an important impact on the stability and recyclability of the composites. Interestingly, Ag NCs/ TiO_2 show distinct performances towards the photocatalytic degradation of rhodamine B (RhB, cationic dye) and MO (anionic dye). Ag NCs/ TiO_2 can significantly degrade RhB, but little effect was observed with respect to MO degradation. This phenomenon can be attributed to the completely opposite electrostatic interactions between the surfaces of Ag NCs/ TiO_2 and these dye molecules. Furthermore, electron paramagnetic resonance (EPR) measurements and scavenger experiments reveal that $\cdot\text{O}_2^-$ radicals are the main active species during the photocatalytic reactions.

2. Experimental

2.1. Preparation of Ag NCs

The preparation process of Ag NCs adopted a previously reported protocol, with some modifications [34]. Typically, 0.06 mL (0.8 M) Poly (methacrylic acid, sodium salt) solution (PMAA) was added into freshly prepared 4.8 mL AgNO_3 (0.05 M) in a 50 mL beaker under stirring. Then the mixture solution was incubated in the dark for 5 min. After that, HNO_3 (0.1 M) was introduced to adjust the pH of the solution to ca. 4.8. After another period of 15 min, above solution was subjected to ultraviolet (UV) irradiation ($\lambda = 365$ nm) for 5 min. The color of the obtained solution is red brown.

2.2. Preparation of Ag NCs/ TiO_2

In a typical procedure, P25 (0.5 g) was dispersed in 50 mL ultrapure water (18.25 $\text{M}\Omega\text{-cm}$), then the mixture was ultrasonicated for 20 min. Followed by introducing different volumes (0.8 mL, 1.6 mL, 2.4 mL) of freshly prepared Ag NCs solution in above mixture. After that, the mixture (contains Ag NCs and TiO_2) was subjected to drastic stirring. This stage lasts for 2 h at room temperature, and then Ag NCs/ TiO_2 powders were gathered by centrifugation (8000 rpm, 15 min) and rotary evaporation at 60 °C. The as-prepared Ag NCs/ TiO_2 showed a light pink color. Ag NCs/ TiO_2 with different Ag/Ti molar ratios of 0.52%, 0.89%, 1.41% (corresponding to 0.8 mL, 1.6 mL, 2.4 mL of Ag NCs solution, respectively) were denoted as Ag NCs/ TiO_2 -0.52, Ag NCs/ TiO_2 -0.89, Ag NCs/ TiO_2 -1.41.

2.3. Characterization

X-ray diffraction (XRD, Bruker D8) was used to identify the crystal structure of obtained samples. Transmission electron microscopy (TEM, JEM-2011) were adopted to observe the morphological photographs of the composite. Brunauer-Emmett-Teller (BET) surface area (S_{BET}) was recorded at 77 K using N_2 adsorption/desorption isotherms (QUADRASORB IQ, Quantachrome Instrument Corp). Samples were degassed at 100 °C for 12 h before the nitrogen adsorption measurements. Optical properties of composite powders were analyzed via ultraviolet-visible diffusion reflectance spectra (UV-vis DRS, Shimadzu SolidSpec-3700 DUV), and BaSO_4 was used as the standard reference. Fluorescence spectra were recorded on a Hitachi F-7000 fluorescence spectrophotometer (the slit width was adjusted to 5 nm during the emission spectra measurement). EPR were measured through Bruker Elexsys E500 spectrometer at room temperature. Inductively coupled plasma optical emission spectrometry (ICP-OES, VISTA-PRO CCD) was used to analyze the Ag/Ti (molar ratio) in Ag NCs/ TiO_2 composite. Absorption measurements of solutions were performed via the UV-vis spectrophotometer (Shimadzu UV-1800, Japan). Zeta potential (ζ) was conducted through a Nano-ZS zetasizer (Malvern Instruments). Specially, Ag NCs/ TiO_2 (2 mg) was dispersed in H_2O (10 mL), and the measurement was performed three times to get the average value. Photocurrent was measured through an electrochemical workstation (CHI 760 E, Chenhua, China).

2.4. Photocatalytic activity tests

The photoactivity of Ag NCs/ TiO_2 composites were assessed by the photocatalytic removal of NO and photocatalytic dye degradation (the detailed process is presented in the supporting information) under visible light irradiation. The light source was supplied by a 300 W xenon lamp incorporated with a band pass filter ($\lambda > 420$ nm). The intensity of the visible light reaches the surface of photocatalysts is 74.12 mW cm^{-2} , as measured by the optical power meter (Model 1918-R, Newport). The lamp was turned on 30 min for stabilization before conducting all the photocatalytic reactions.

Photocatalytic removal of NO was performed on a NO analyzer (Thermo Environmental Instrument Inc. Model 42i). The detection limit of the instrument ranges from sub-ppm up to ppm levels. Before the test, 50 mg of photocatalysts were put into a beaker (50 mL). And then H_2O (10 mL) was introduced into the beaker and the mixture was ultrasonicated vigorously till photocatalysts were uniformly dispersed. After a period of about 20 min, the above mixture was gently poured into a glass dish (whose diameter is 6.4 cm), followed by drying in a vacuum drying oven for 8 h. After that, the dish was put into a reactor, whose volume is about 0.785 L ($\pi \times 5^2 \text{ cm}^2 \times 10 \text{ cm}$). During the test, air stream was used to dilute the concentration of NO to about 600 ppb. After reaching a state of equilibrium (the concentration of NO did not show any changes), the lamp was placed to the top of the reactor for irradiation.

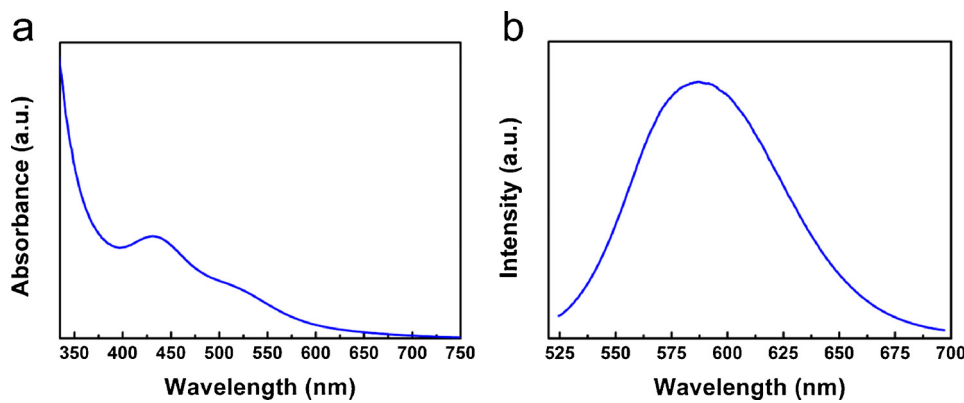


Fig. 1. (a) UV-vis absorption spectrum and (b) photoluminescence (PL) emission spectrum of as-prepared Ag NCs solution (the excitation wavelength is 505 nm).

The removal rate of NO was obtained by the following formula:

$$\text{NO removal rate (\%)} = (C_0 - C)/C_0 \times 100\%,$$

where C and C_0 refer to the NO concentration at a given time and the initial concentration of NO, respectively.

3. Results and discussion

3.1. Characterization of as-prepared materials

UV-vis absorption spectrum, as presented in Fig. 1a, shows the optical property of Ag NCs. Ag NCs exhibit multiple absorption bands, at 430 nm and about 500 nm. Besides, the plasmon absorption located from 380 to 420 nm for Ag NPs cannot be observed in the spectrum, indicating the formation of NCs rather than NPs [35]. Typically, these characteristic absorption bands can be attributed to the features of Ag NCs obtained through photoreduction [36,37]. Furthermore, the absence of surface-plasmon absorption indicates nonmetallic nature (or quantum-dot behavior) of Ag NCs. Interestingly, these Ag NCs exhibit an absorption tail, which can be observed in semiconductors [38]. Besides, the emerging strong fluorescence due to the discrete electronic states is a significant feature of ultra-small clusters, which cannot be found in NPs [39]. As shown in Fig. 1b, a notable PL emission peak located at about 590 nm is observed upon the excitation. The absorption and emission properties support the successful preparation of ultra-small Ag clusters. And these Ag NCs with molecular like properties can act as a kind of potential photocatalyst, similar to semiconductor photocatalysts.

In addition, Ag NCs were supported on TiO_2 to improve their recyclability and stability. The phase composition and crystal structure of

the powder composites were identified by XRD. Fig. 2a shows the characteristic diffraction peaks of anatase and rutile, where peaks marked by red quadrangles are assigned to anatase (JCPDF#71-1166), while those signed by red solid dots represent rutile (JCPDF#73-1763). Besides, no diffraction peaks belong to Ag NCs are found in the Ag NCs/ TiO_2 composite, because of the low content of Ag. HRTEM was conducted to reveal the morphologies of the as-prepared Ag NCs/ TiO_2 -0.89. As shown in Fig. 2b, the ultra-small Ag NCs are basically monosized (marked by red circles), at about 1.5 nm and the interplanar distance of ca. 0.35 nm is assigned to the (101) plane of anatase phase TiO_2 [40]. Note that these relative bigger Ag NCs are formed through aggregation because of the electron beam irradiation. Generally, this susceptibility to electron beam has been reported in many literatures, which is often observed in Ag NCs-based system [33,41]. It is commonly accepted that Ag NPs lose SPR effect when their sizes are smaller than 2 nm, and this is consistent with the result of UV-vis spectral observation.

3.2. Photocatalytic removal of NO

Photocatalytic removal of NO under visible light was used to evaluate the redox properties of the as-prepared Ag NCs/ TiO_2 composites. Typically, blank tests evidence that the removal of NO could not occur in the absence of light irradiation or photocatalysts. As shown in Fig. 3a, TiO_2 and Ag NCs all show a relative small ability towards the removal of NO; the NO removal rate reaches at about 22% and 32% after 22 min, respectively. By contrast, the removal percentages of NO for Ag NCs/ TiO_2 are all higher than that of TiO_2 and Ag NCs, due to the fast carriers separation in Ag NCs/ TiO_2 composites. Ag NCs/ TiO_2 -0.52 can remove about 45% of NO, which is about 2 times and 1.4 time

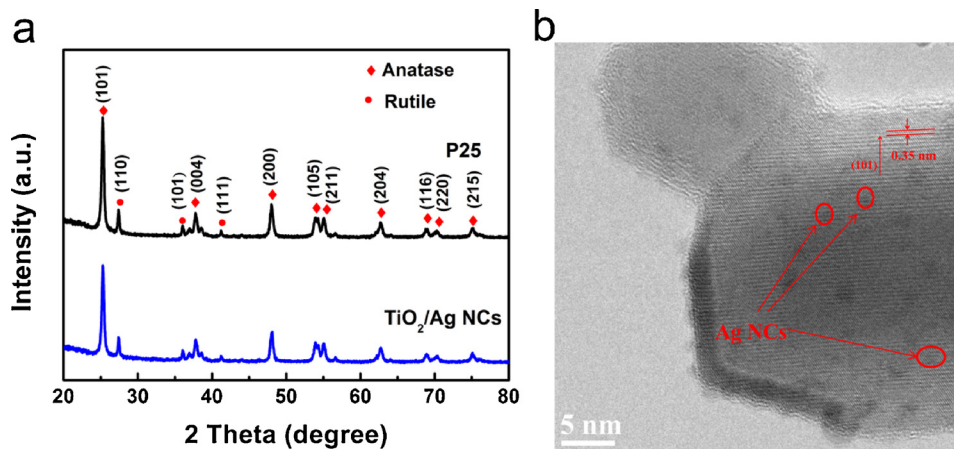


Fig. 2. (a) The XRD pattern and (b) HRTEM image of Ag NCs/ TiO_2 -0.89.

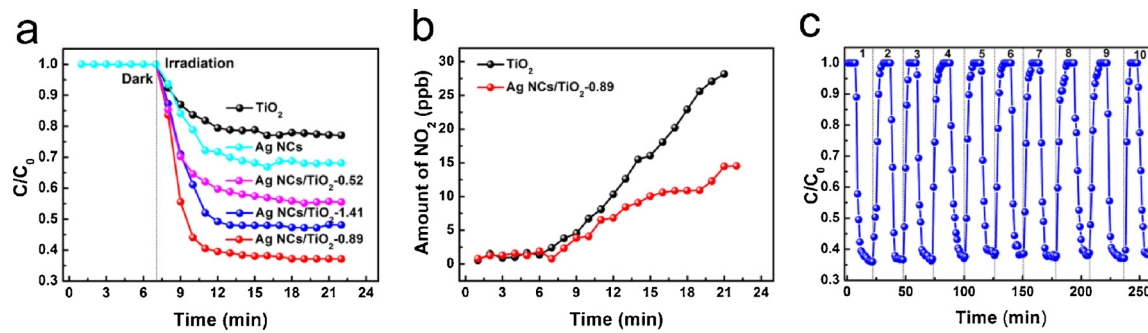


Fig. 3. (a) Photocatalytic removal of NO for TiO_2 , Ag NCs, $\text{Ag NCs/TiO}_2\text{-}0.52$, $\text{Ag NCs/TiO}_2\text{-}0.89$, and $\text{Ag NCs/TiO}_2\text{-}1.4$ under visible light ($\lambda > 420 \text{ nm}$); (b) The formed amount of NO_2 over the pristine TiO_2 and $\text{Ag NCs/TiO}_2\text{-}0.89$ during reactions; (c) The photocatalytic stability test in 10 cycles for $\text{Ag NCs/TiO}_2\text{-}0.89$.

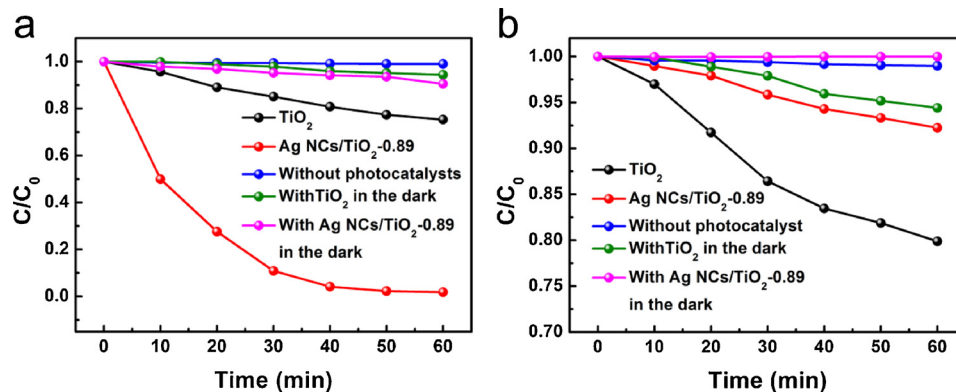


Fig. 4. Photocatalytic degradation of (a) RhB and (b) MO under visible light using different photocatalysts.

higher than the TiO_2 and Ag NCs. Furthermore, $\text{Ag NCs/TiO}_2\text{-}0.89$ have better photoactivity than $\text{Ag NCs/TiO}_2\text{-}0.52$. More than 60% of NO is converted in just 5 min after irradiation. The percentage of NO removed by $\text{Ag NCs/TiO}_2\text{-}0.89$ is 63%, which is about 3 times and 2 times as high as that by the bare TiO_2 and Ag NCs respectively. The photoactivity towards the NO removal slightly declines as the loading amount of Ag is further increased. With respect to $\text{Ag NCs/TiO}_2\text{-}1.4$, the removal rate of NO is 52%. As presented in the TEM image of $\text{Ag NCs/TiO}_2\text{-}1.4$ (Fig. S1), some aggregation of Ag NCs can be observed as the loading amount of Ag is further increased. The aggregation decreases the amount of active sites on Ag NCs as well as on TiO_2 . Besides, these aggregated Ag NCs cannot efficiently transfer photogenerated electrons to TiO_2 , and therefore the photoactivity of NO removal slightly declines.

We also recorded the formed amount of the intermediate product, NO_2 (which is more toxic than NO) for TiO_2 and $\text{Ag NCs/TiO}_2\text{-}0.89$. Interestingly, the amount of NO_2 produced by TiO_2 is consistently higher than that of $\text{Ag NCs/TiO}_2\text{-}0.89$ (Fig. 3b). Over a period of about 20 min, the production of NO_2 for $\text{Ag NCs/TiO}_2\text{-}0.89$ is 13 ppb, compared to that of about 28 ppb for TiO_2 . This result indicates that Ag NCs play a key role in inhibiting the formation of NO_2 . Typically, this phenomenon could be ascribed to two aspects. First, similar to previous reports that BaO species [42] and STO matrix [43] could act as the NO_x storage material, the Ag NCs may also have the ability of efficiently storing NO_x and inhibiting the emission of NO_2 . Second, the supported Ag NCs increase the number of active sites and therefore the separation of photogenerated carriers, which facilitates the further oxidation of NO_2 to form other species, like HNO_2 and HNO_3 [44]. Besides, the amount of formed NO_2 is considerably lower than that of removed NO (about 138 and 320 ppb for the bare TiO_2 and $\text{Ag NCs/TiO}_2\text{-}0.89$, respectively), implying that the majority of the NO is oxidized to NO_3^- or other forms of nitric oxides.

The recyclability and stability of $\text{Ag NCs/TiO}_2\text{-}0.89$ were further explored. It is clear from Fig. 3c that the photoactivity of $\text{Ag NCs/TiO}_2\text{-}0.89$ does not show any upward trend even after 10 continuous test

cycles. The removal percentage of NO retains at about 63% for every cycle, with little fluctuation. The significant removal of NO retains suggests that Ag NCs can act as a semiconductor and transfer excited electrons to TiO_2 , and then NO is gradually oxidized. On the other hand, this exciting phenomenon also proves the essential role of supports in metal NCs/supports system for photocatalysis. We will discuss the specific reaction mechanism in more detail later.

3.3. Selective photocatalytic dyes degradation

With respect to the photocatalysis, metal NCs have been extensively used in the degradation of dyes [6,19,35,45]. In this study, we applied TiO_2 and $\text{Ag NCs/TiO}_2\text{-}0.89$ to the photocatalytic degradation of RhB under visible light. We aim at the further exploration of the photocatalytic performance of Ag NCs/TiO₂, and finding some commonness and differences during photocatalytic removal of NO and dyes degradation. As shown in Fig. 4a, the photoactivity of RhB degradation for $\text{Ag NCs/TiO}_2\text{-}0.89$ is significantly higher than that of TiO_2 . After a period of 40 min irradiation, the concentration of Rh B drops to about 0.02%, while the decomposition ratio for TiO_2 is only 20% within the same time frame. For the pristine TiO_2 , the value of decomposition ratio is only about 24% after the irradiation of 1 h. The result suggests that small loading amount of Ag NCs can noticeably enhance the photoactivity of TiO_2 , bringing about 5 times increase in photocatalytic performance for $\text{Ag NCs/TiO}_2\text{-}0.89$ composite. By contrast, the concentration of RhB falls by about 1.1% in the absence of photocatalysts, indicating RhB is a kind of stable molecule and its photolysis is ignorable. Besides, the concentrations of RhB for TiO_2 and $\text{Ag NCs/TiO}_2\text{-}0.89$ without light irradiation do not show any significant changes, suggesting these reactions are definitely driven by light.

Moreover, we explored the decomposable ability of $\text{Ag NCs/TiO}_2\text{-}0.89$ towards another kind of dye, MO (Fig. 4b). Surprisingly, after being exposed to visible light irradiation for 60 min, the concentration of MO over $\text{Ag NCs/TiO}_2\text{-}0.89$ drops by only 8%, compared to 20% in

the decomposition ratio of MO over TiO_2 . Similarly, when TiO_2 or Ag NCs/ TiO_2 -0.89 being kept in the dark, or MO is irradiated without photocatalysts, the concentration of MO decreases slightly (all less than 5%).

We attribute the distinct photocatalytic performances of Ag NCs/ TiO_2 towards these two kinds of dyes to electrostatic interaction at the photocatalysts/dyes surface. As reported previously, cationic dyes can be significantly adsorbed by electronegative clusters because of the electrostatic attraction, while anionic dyes cannot due to the strong electrostatic repulsion [33]. The value of Zeta potential for Ag NCs/ TiO_2 -0.89 is -12.4 mV (negative). As photogenerated carriers transfer on the surfaces of photocatalysts during photocatalytic reactions, the adsorption process is essential. Dyes cannot be degraded unless they are adsorbed by the photocatalyst. Typically, it is almost impossible for the anionic dye, MO, to be adsorbed by the electronegative Ag NCs/ TiO_2 , thus subsequent reactions fail to happen. However, RhB, a kind of cationic dyes, can be efficiently adsorbed, and then gradually being removed by Ag NCs/ TiO_2 .

The reaction pattern is further enlarged to another kind of cationic dye, MB, to validate the selectivity of degradation reactions photocatalyzed by the Ag NCs/ TiO_2 -0.89 (chemical structures of Rh B, MB, and MO are shown in Fig. S2). Similarly, the concentration of MB drops to only 2% after the illumination of 1 h (Fig. S3). These results demonstrate that Ag NCs/ TiO_2 -0.89 can selectively degrade cationic dyes.

3.4. Analyses of photocatalytic mechanism and photoactivity enhancement

Fig. 5a exhibits the UV–vis DRS spectrum of Ag NCs/ TiO_2 -0.89. After Ag NCs are loaded on the surface of TiO_2 , obvious red shift of the absorption is observed. Typically, absorption bands at 496 nm and 545 nm emerge, corresponding to 430 nm and 500 nm bands in the unsupported Ag NCs (Fig. 1), respectively. Note that the slight red shift can be attributed to the close interaction between TiO_2 and Ag NCs [6]. Besides, UV–vis DRS spectrum of Ag NCs/ TiO_2 -0.89 also proves that the composite can significantly absorb visible light because of the introduced Ag NCs. And it is reasonable that Ag NCs/ TiO_2 -0.89 exhibits improved photoactivity towards the removal of NO and the degradation of cationic dyes. With respect to the photon energy scale, two bands located at about 2.27 eV and 2.50 eV (Fig. 5b).

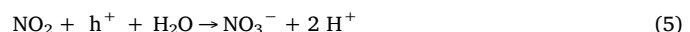
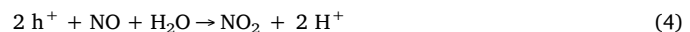
EPR was conducted to explore the active species involved in the photocatalysis. As shown in Fig. 6a, four characteristic peaks with relative intensities of about 1:1:1:1 are clearly observed for Ag NCs/ TiO_2 -0.89, suggesting the formation of $\cdot\text{O}_2^-$ radicals during irradiation [46,47]. And the other two peaks for Ag NCs/ TiO_2 -0.89 belong to the hyperfine splitting peaks for the superoxide/DMPO adduct, these peaks have also been reported by many previous articles [43,47,48]. However, no obvious signal of $\cdot\text{O}_2^-$ radicals can be tracked for TiO_2 . On the other hand, $\cdot\text{OH}$ radicals do not participate in the photocatalytic reactions, as confirmed by the absence of the specific EPR signals when

replacing the methanol solution with aqueous solution (Fig. 6b).

The scavenger experiments were also performed and shown in Fig. 7. In this work, KI, AgNO_3 , p-Benzoquinone (PBQ), and tert-Buanol (TBA) were used as the scavengers for photogenerated holes, photogenerated electrons, $\cdot\text{O}_2^-$ radicals, and $\cdot\text{OH}$ radicals, respectively. The photocatalytic performance of Ag NCs/ TiO_2 -0.89 towards the removal of NO declines significantly after the addition of KI, AgNO_3 , and PBQ, indicating that photogenerated holes and photogenerated electrons (photogenerated carriers), as well as $\cdot\text{O}_2^-$ radicals are responsible for the photocatalytic reactions. However, the photoactivity of the sample does not show any apparent changes when TBA is introduced, suggesting that $\cdot\text{OH}$ radicals are not involved in the current reaction. And these results are well matched with the EPR result.

Based on above results and discussion, processes of charges transfer and radicals generation at the surface of Ag NCs/ TiO_2 composite are proposed and illustrated in Fig. 8. In the present system, $\cdot\text{OH}$ radicals were not detected under visible light, suggesting that the highest occupied molecular orbital (HOMO) level of Ag NCs is more negative than both 1.99 eV for $\text{OH}^-/\cdot\text{OH}$ and 2.37 eV for $\text{H}_2\text{O}/\cdot\text{OH}$. Meanwhile, the lowest unoccupied molecular orbital (LUMO) level of Ag NCs is more negative than the standard redox potential of -0.33 eV for $\text{O}_2/\cdot\text{O}_2^-$ on the basis of the EPR results. Therefore, it is reasonable to reckon that the LUMO level of Ag NCs lies more negative than the CB potentials of both rutile and anatase, thus photogenerated electrons can significantly transfer from Ag NCs to TiO_2 under visible light irradiation.

Herein, the underlying processes for photocatalytic removal of NO are presented. First, photoinduced carriers appear because of the incident light (1). Photogenerated electrons directly react with O_2 from the air to form $\cdot\text{O}_2^-$ radicals (2). Then $\cdot\text{O}_2^-$ radicals contribute to the oxidation of NO, forming NO_3^- (3). Meanwhile, NO is oxidized by photogenerated holes to other nitrogen oxides step by step (reactions 4–6).



In these cycles, photocatalytic reactions happen with the assistance of $\cdot\text{O}_2^-$ radicals and photogenerated carriers over Ag NCs/ TiO_2 under visible light irradiation.

Moreover, Ag NCs/ TiO_2 -0.89 shows notably higher photocurrent density than the pristine TiO_2 (Fig. 9), indicating improved interfacial charges transfer efficiency [28,49]. The result is consistent with the enhanced photocatalytic performance for Ag NCs/ TiO_2 -0.89. However,

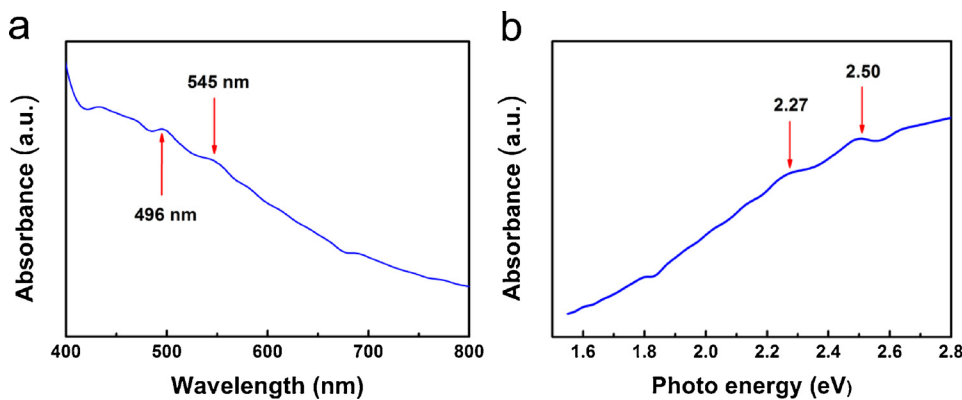


Fig. 5. (a) UV–vis DRS spectrum of Ag NCs/ TiO_2 -0.89; (b) The absorption spectrum versus photon energy scale.

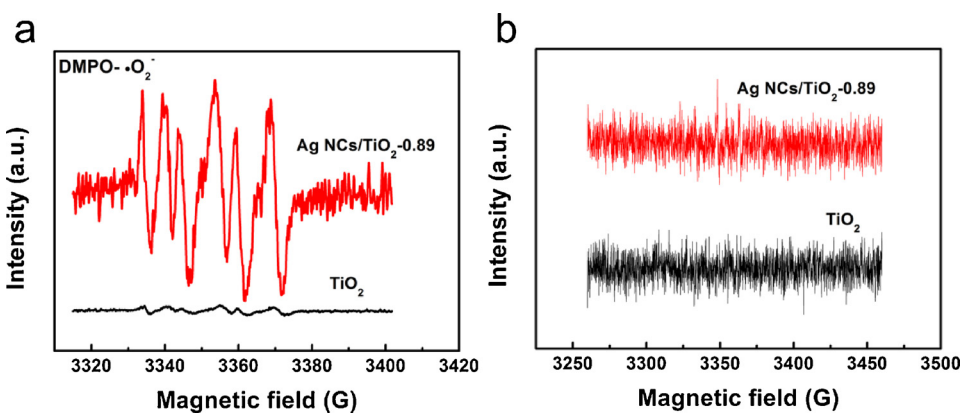


Fig. 6. EPR spectra of Ag NCs/TiO₂-0.89 and TiO₂, measured at $\lambda > 420$ nm after being exposed to illumination for 5 min, using (a) the methanol solution and (b) the aqueous solution of 5,5-Dimethyl-1-pyrrolineN-oxide (DMPO) as the trapping agent.

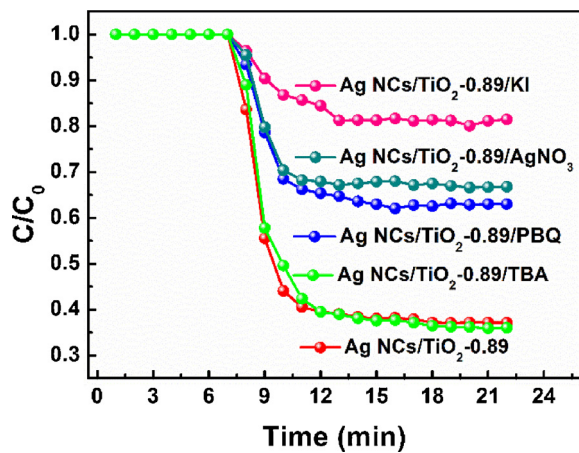


Fig. 7. The scavenger experiments of photocatalytic NO removal for the Ag NCs/TiO₂-0.89. KI, AgNO₃, PBQ, and TBA were used as the photogenerated holes, photogenerated electrons, ·O₂[−] radicals, and ·OH radicals scavengers, respectively.

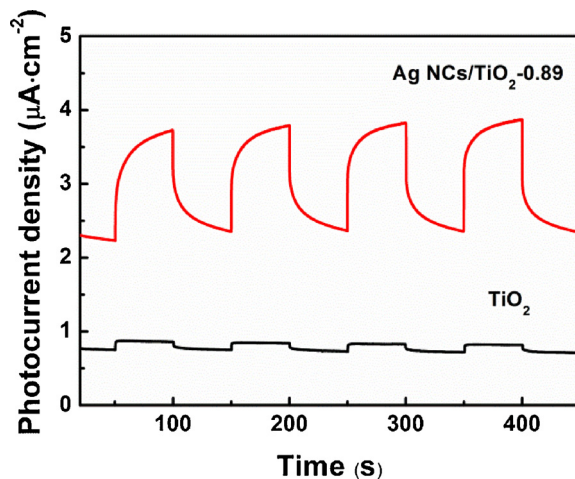


Fig. 9. Photocurrent–time curves of Ag NCs/TiO₂-0.89 and TiO₂ under visible-light irradiation.

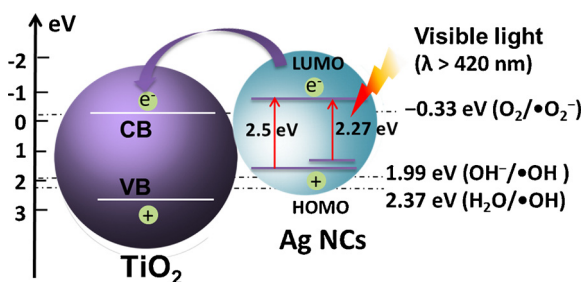


Fig. 8. Schematic illustration of charges transfer and radicals generation over Ag NCs/TiO₂ composite.

the gap between surface areas of Ag NCs/TiO₂-0.89 ($54 \text{ m}^2 \text{ g}^{-1}$) and TiO₂ ($58 \text{ m}^2 \text{ g}^{-1}$) is very narrow (Fig. S4). This is due to the very low loading amount of Ag NCs on the surface of TiO₂.

Taken together, above results support that small amount of Ag NCs loaded on TiO₂ can considerably promote the separation of photogenerated carriers and induce the formation of ·O₂[−] radicals, which largely enhance the photoactivity of the composite under visible light.

4. Conclusions

In summary, Ag NCs/TiO₂ composites were successfully prepared through the deposition of Ag NCs solutions. HRTEM results show that the size of Ag NCs is smaller than 2 nm. We also investigated the

photocatalytic performances of Ag NCs/TiO₂ composites. Small loading amount of Ag NCs (0.89% in Ag/Ti molar ratio) provides great potential for photocatalysis. The photoactivity of NO removal over Ag NCs/TiO₂-0.89 is about 3 times and 2 times as high as that of the bare TiO₂ and Ag NCs, respectively. More importantly, Ag NCs/TiO₂-0.89 can efficiently inhibit the formation of NO₂, and the composite shows extraordinary stability during 10 cycling tests. In addition, Ag NCs bring about a 5 times increase in photocatalytic degradation of RhB, but about 2 times decrease for the degradation of MO. The distinct photocatalytic performances are attributed to different electrostatic interactions at the photocatalyst/dyes surface. Moreover, we have shown that Ag NCs can work as a semiconductor, which can be excited by the incident light, and then transfer electrons to TiO₂ and facilitate the separation of photogenerated electron-hole pairs. ·O₂[−] radicals are the main active species involved in the photocatalytic reactions, as proved by EPR results and scavenger experiments. Future work should be conducted to explore the specific composition and structure of Ag NCs, and further probe the effects of different number of Ag atoms on photocatalytic performances.

Conflicts of interest

There are no conflicts of interest to declare.

Acknowledgments

Financial support by the National Natural Science Foundation of

China (Grant No. 21473248), the Guangdong Provincial Science and Technology Project (2017A050506009), and the Support Scheme of Guangzhou for Leading Talents in Innovation and Entrepreneurship funding from Guangzhou (No. 2016015) is gratefully appreciated.

Appendix A. Supplementary data

Supplementary material related to this article can be found, in the online version, at doi:<https://doi.org/10.1016/j.apcatb.2018.04.041>.

References

- [1] Y. Chen, Y. Wang, W. Li, Q. Yang, Q. Hou, L. Wei, L. Liu, F. Huang, M. Ju, *Appl. Catal. B: Environ.* 210 (2017) 352–367.
- [2] W. Fan, C. Chen, H. Bai, B. Luo, H. Shen, W. Shi, *Appl. Catal. B: Environ.* 195 (2016) 9–15.
- [3] X. Chen, Y. Li, X. Pan, D. Cortie, X. Huang, Z. Yi, *Nat. Commun.* 7 (2016) 1–8.
- [4] Y. Duan, S. Zhou, Z. Chen, J. Luo, M. Zhang, F. Wang, T. Xu, C. Wang, *Catal. Sci. Technol.* 8 (2018) 1395–1403.
- [5] Z. Bian, T. Tachikawa, P. Zhang, M. Fujitsuka, T. Majima, *J. Am. Chem. Soc.* 136 (2014) 458–465.
- [6] C. Yu, G. Li, S. Kumar, H. Kawasaki, R. Jin, *J. Phys. Chem. Lett.* 4 (2013) 2847–2852.
- [7] C.C. Huang, Z. Yang, K.H. Lee, H.T. Chang, *Angew. Chem. Int. Ed.* 119 (2007) 6948–6952.
- [8] Y.-C. Shiang, C.-C. Huang, W.-Y. Chen, P.-C. Chen, H.-T. Chang, *J. Mater. Chem.* 22 (2012) 12972–12982.
- [9] J. Yu, S.A. Patel, R.M. Dickson, *Angew. Chem. Int. Ed.* 119 (2007) 2074–2076.
- [10] Z. Wu, D.E. Jiang, A.K. Mann, D.R. Mullins, Z.A. Qiao, L.F. Allard, C. Zeng, R. Jin, S.H. Overbury, *J. Am. Chem. Soc.* 136 (2014) 6111–6122.
- [11] X. Nie, H. Qian, Q. Ge, H. Xu, R. Jin, *ACS Nano* 6 (2012) 6014–6022.
- [12] W. Chen, S. Chen, *Angew. Chem. Int. Ed.* 48 (2009) 4386–4389.
- [13] G. Kwon, G.A. Ferguson, C.J. Heard, E.C. Tyo, C. Yin, J. DeBartolo, S. Seifert, R.E. Winans, A.J. Kropf, J. Greeley, *ACS Nano* 7 (2013) 5808–5817.
- [14] M. Turner, V.B. Golovko, O.P. Vaughan, P. Abdulkin, A. Berenguer-Murcia, M.S. Tikhov, B.F. Johnson, R.M. Lambert, *Nature* 454 (2008) 981–983.
- [15] S. Zhou, Y. Duan, F. Wang, C. Wang, *Nanoscale* 9 (2017) 4981–4988.
- [16] N. Sakai, T. Tatsuma, *Adv. Mater.* 22 (2010) 3185–3188.
- [17] A. Kogo, N. Sakai, T. Tatsuma, *Electrochem. Commun.* 12 (2010) 996–999.
- [18] H. Zhang, X. Li, G. Chen, *J. Mater. Chem.* 19 (2009) 8223.
- [19] K. Sridharan, E. Jang, J.H. Park, J.H. Kim, J.H. Lee, T.J. Park, *Chem. Eur. J.* 21 (2015) 9126–9132.
- [20] P. Forzatti, *Appl. Catal. A: Gen.* 222 (2001) 221–236.
- [21] J. Lasek, Y.-H. Yu, J.C. Wu, *J. Photoch. Photobio. C: Photoc. Rev.* 14 (2013) 29–52.
- [22] W.-F. Yang, H.-J. Hsing, Y.-C. Yang, J.-Y. Shyng, J. Hazard. Mater. 148 (2007) 653–659.
- [23] S. Bröer, T. Hammer, *Appl. Catal. B: Environ.* 28 (2000) 101–111.
- [24] J. Ma, C. Wang, H. He, *Appl. Catal. B: Environ.* 184 (2016) 28–34.
- [25] X. Ding, W. Ho, J. Shang, L. Zhang, *Appl. Catal. B: Environ.* 182 (2016) 316–325.
- [26] W. Zhu, P. Liu, S. Xiao, W. Wang, D. Zhang, H. Li, *Appl. Catal. B: Environ.* 172–173 (2015) 46–51.
- [27] J. Ma, H. He, F. Liu, *Appl. Catal. B: Environ.* 179 (2015) 21–28.
- [28] Y. Duan, M. Zhang, L. Wang, F. Wang, L. Yang, X. Li, C. Wang, *Appl. Catal. B: Environ.* 204 (2017) 67–77.
- [29] Z. Zhao, W. Zhang, X. Lv, Y. Sun, F. Dong, Y. Zhang, *Environ. Sci.: Nano* 3 (2016) 1306–1317.
- [30] X. Feng, W. Zhang, Y. Sun, H. Huang, F. Dong, *Environ. Sci.: Nano* 4 (2017) 604–612.
- [31] M.M. Khin, A.S. Nair, V.J. Babu, R. Murugan, S. Ramakrishna, *Energy Environ. Sci.* 5 (2012) 8075–8109.
- [32] L. Zhou, C. Gao, W. Xu, A.C.S. Appl. Mater. Inter. 2 (2010) 1483–1491.
- [33] M.S. Bootharaju, T. Pradeep, *Langmuir* 29 (2013) 8125–8132.
- [34] L. Shang, S. Dong, *Chem. Commun.* (2008) 1088–1090.
- [35] W.T. Chen, Y.J. Hsu, P.V. Kamat, *J. Phys. Chem. Lett.* 3 (2012) 2493–2499.
- [36] J. Zheng, R.M. Dickson, *J. Am. Chem. Soc.* 124 (2002) 13982–13983.
- [37] J. Zhang, S. Xu, E. Kumacheva, *Adv. Mater.* 17 (2005) 2336–2340.
- [38] J. Schneider, M. Matsuoka, M. Takeuchi, J. Zhang, Y. Horiuchi, M. Anpo, D.W. Bahnemann, *Chem. Rev.* 114 (2014) 9919–9986.
- [39] J. Zheng, C. Zhang, R.M. Dickson, *Phys. Rev. Lett.* 93 (2004) 077402.
- [40] D. Ding, K. Liu, S. He, C. Gao, Y. Yin, *Nano Lett.* 14 (2014) 6731–6736.
- [41] T.U.B. Rao, B. Nataraju, T. Pradeep, *J. Am. Chem. Soc.* 132 (2010) 16304–16307.
- [42] A. Yamamoto, Y. Mizuno, K. Teramura, S. Hosokawa, T. Tanaka, *Appl. Catal. B: Environ.* 180 (2016) 283–290.
- [43] Q. Zhang, Y. Huang, L. Xu, J.-j. Cao, W. Ho, S.C. Lee, *ACS Appl. Mater. Inter.* 8 (2016) 4165–4174.
- [44] Z. Zhang, M. Xu, W. Ho, X. Zhang, Z. Yang, X. Wang, *Appl. Catal. B: Environ.* 184 (2016) 174–181.
- [45] N. Vilar-Vidal, J.R. Rey, M.A. Lopez Quintela, *Small* 10 (2014) 3632–3636.
- [46] W. He, H.K. Kim, W.G. Wamer, D. Melka, J.H. Callahan, J.J. Yin, *J. Am. Chem. Soc.* 136 (2014) 750–757.
- [47] H. Jia, W. He, W.G. Wamer, X. Han, B. Zhang, S. Zhang, Z. Zheng, Y. Xiang, J.-J. Yin, *J. Phys. Chem. C* 118 (2014) 21447–21456.
- [48] H. Zhao, J. Joseph, H. Zhang, H. Karoui, B. Kalyanaraman, *Free Radic. Bio. Med.* 31 (2001) 599–606.
- [49] M. Zhang, Y. Duan, H. Jia, F. Wang, L. Wang, Z. Su, C. Wang, *Catal. Sci. Technol.* 7 (2017) 452–458.